ISSN 1070-3632, Russian Journal of General Chemistry, 2008, Vol. 78, No. 4, pp. 704–722. © Pleiades Publishing, Ltd., 2008.
Original Russian Text © A.N. Isaev, 2007, published in Rossiiskii Khimicheskii Zhurnal, 2007, Vol. 51, No. 5, pp. 34–48.

Cooperative Interactions of Hydrogen Bonds in Proton-Transfer Processes Involving Water Molecules. Simulation of Biochemical Systems

A. N. Isaev

Zelinskii Institute of Organic Chemistry, Russian Academy of Sciences, Leninskii pr. 47, Moscow, 119991 Russia
e-mail isaevaln@ioc.ac.ru

Received July 26, 2007

Abstract–Quantum-chemical calculations of molecular complexes simulating the proton channel of influenza A virus and the proton-transfer system of the active site of carboanhydrase enzyme were performed. These complexes comprise a proton-donor and a proton-acceptor groups bridged by a chain of water molecules. Calculations of the methylimidazole (H^+)–H_2O–CH_3COO^- complex as a model of influenza M_2 virus revealed free translation motion of the water molecule between the donor and acceptor, as well as concerted proton transfer in both H bonds. The barrier for proton transfer is independent of the position of the bridging water molecule and varies linearly with the difference in the electrostatic potentials between the donor and acceptor. With elongation of the H-bond bridge between the donor and acceptor groups, the H-bond lengths and proton shifts in the chain links vary periodically. This process can be defined as an H-bond deformation wave (proton wave). It was shown that motion of one proton along the H bond is associated with vibrational motion of protons in other links, which results in wave propagation along the chain. The calculation results allowed the rate of the proton wave and the time of proton transfer from the donor to acceptor to be estimated.

DOI: 10.1134/S1070363208040324

Role of Hydrogen Bonds and Water Molecules in Enzymatic Catalysis

Hydrogen bonds play an important role in enzymatic catalysis. Evidence for this conclusion was obtained in 1990s in experiments on mutagenesis (see, for example, [1, 2]), which revealed stabilization of the transition state in the active site of an enzyme on enzyme–substrate hydrogen bonding. Theoretical studies on model systems [3–5] showed that hydrogen bonding can contribute much in the catalytic activity of enzymes. Thus a quantum-chemical study [4] of the mechanism of stabilization of the transition state of the reaction in the active site of papain cystein protease allowed the acceleration of the hydrolysis of the peptide nitrile under the action of the mutated enzyme to be explained in terms of hydrogen bonding in the transition state.

Active sites of enzymes feature the presence of a structurally flexible net of H bonds between functionally active groups of the enzyme, the substrate, and water molecules contained in the active site. Thus Hoog et al. [6] found in the crystal structure of the HSV-2 serine protease/inhibitor complex a net of H bonds between amino acid residues of the enzyme, covalently bound ligand, and central water molecules. The principal elements of the active site of this enzyme are surprisingly closely similar to those in chemotripsin, even though these enzymes do not have a homologous sequence and have quite different quaternary structures. These findings provide evidence for the suggestion that these enzymes act by a common mechanism, even though catalysis involves different amino acid residues.

In certain sites of proteins, internal water clusters form H bonds with surrounding water molecules, thus providing binding between the internal part of the protein and its water surrounding. Thus, the molecular graphical analysis of the X-ray data for the active site of Mo-nitrogenase enzyme [7] revealed two H-bond nets that bind the active site with the outer surface of the protein. Internal water channels allow water molecules to diffuse into the reaction site of the enzyme, which is located in the depth of the molecule [8]. The geometry of the internal channel can allow for several water molecules to form an H-bond chain [9]. Evidence for the existence of a water bridge between

the active site and the protein surface was obtained in the research on cytochrome P450 monooxygenase [10]. According to the proposed two-state model, change in the conformation of the monooxigenase arginine give rise to formation of a functional water channel from the active site to a water cluster located on the thiolate side of the heme, close to the protein surface. This water cluster communicates with the surface in the closed state and is partly replaced by the flipping arginine side chain in the open state, allowing water molecules to exit to the surface or to reaccess the active site.

Over late 1990s a lot of interesting data showing that water molecules in the active site of an enzyme can be directly involved in enzymatic catalysis [11–15]. For example, a theoretical study [13] showed that the H bonding between the Thr-218 residue and a water molecule can play a key role in the nucleophilic attack in the active site of aspartate proteinase. The water molecule H-bonded with Tyr-244 and His-290 in the active site of cytochrome *c* oxidase takes part in the proton transfer to Fe–O-–O to form Fe–O–O–H[15].

Proton Transfer in Biomolecules

Extended chains of water molecules, that bridge the active site of an enzyme with solvent, intrinsic water phase of the enzyme, or spatially remote functional groups, can form proton-transfer channels ("proton helix") [16–20]. Along with water molecules, certain amino acid residues, too, can take part in proton transfer [17, 21].

Proton transfer over considerable distances occurs in many biochemical systems. The well-known examples of proton-transfer systems include bacteriorodopsin [22], cytochrome *c* oxidase [23], adenosine 5'-triphosphate (ATP) synthetase [24] and photosynthetic reaction center [25]. Among other interesting systems we can mention the transmembrane channel formed by gramicidin [26] and such enzymes as carboanhydrase [27] and alcohol dehydrogenase [28].

Over the past years the mechanism of proton translocation and the functional role of proton channels have been intensely studied. In particular, experiments with mutated enzymes provide valuable information on the way of proton transfer and not infrequently reveal quite an intricate picture [17]. Thus, in experiments on site-directed mutagenesis with copper–geme oxidases (cytochrome *c*), two channels (D and K) were found. The channel D is used to transport protons involved in the conversion of Fe–O–O to Fe–O–OH, whereas the channel K is responsible for proton loading of the enzyme at some early stages of the catalytic cycle [29]. It was also shown that the rate of electron transfer in oxidases is controlled by proton transfer (proton pump) [30].

Quantum-chemical calculations of model systems prototyping real proton-transfer systems provide information unavailable by experiment and complementing experimental data. Most recent theoretical works on proton-transfer reactions in isolated and solvated H-bonded clusters focused on short chains of H-bonded molecules with an excess proton. In these research, certain constraints were imposed on model molecular systems, with the aim to preserve a quasi-linear chain. In certain works, empiric potentials were used [18, 31]. Many of such works (for example, [32–35]) were based on an original or a modified empirical valence bond (EVB) approximation [36]. Other works made use of quantum dynamics [37, 38] or a combined quantum mechanics and molecular mechanics method [39, 40].

Of interest are approaches that simulate water chains directly inside ionic channels, with calculation of their molecular structure. Thus, Sagnella et al. [41] employed molecular dynamics to simulate the $(H_2O)_5H^+$ cluster built in a polyglycine channel containing thirteen Gly residues and right-turned β helix 10 Å in diameter. As shown in the cited work, the transition complex H_5O^{2+} is readily formed inside the channel, and proton transfer is associated with H bonding of this transition complex with both neighboring water molecules inside the channel and the carbonyl oxygen of glycine in the channel frame.

Classical molecular dynamics was used to simulate a system comprising a gramicidin polypeptide channel, a chain of 10 water molecules built-in inside the channel, and two cylindrical caps of water molecules located outside the channel entrance [42]. Protein–protein interactions were described in terms of the CHARMM force field, whereas the water chain was simulated by means of the empirical Stillinger force field. Appreciable effect of H bonding between the channel and water molecules on proton translocation was observed.

Smondyrev and Voth [43] described interactions between solvated proton and influenza A virus M2 channel surrounding in terms of the EVB model. Molecular dynamics simulation revealed ability of the

excess proton to pass through a ring of gystidine residues by "jumping" between water molecules. The referees concluded that proton diffusion in the channel can correlate with channel conformation. Nemukhin et al. [44] performed a more detailed study of interactions of water molecules of the proton channel with its molecular walls containing His and Asp side chains and simulating the polypeptide surrounding of ionic channels at different stages of proton transfer.

One of the topical problems discussed over the years is whether proton transfer along the H-bond chain occurs via a concerted mechanism or this is a multistage reaction? Unfortunately, neither experiment nor theoretical methods can give an unequivocal answer on this question. The reason is the large size of the molecular system, which creates serious problems in interpreting the results of both measurements of kinetic isotope effects for reactions that occur in the active site of enzymes and high-level quantum-chemical calculations (post-SCF). Even though kinetic isotope effects can provide information on the structure of transition states in short-range proton-transfer reactions [45], isotope effects for long-range proton transfer are quite difficult to interpret because of the great number atoms involved in the process [46].

According to calculations, the "observed" mechanism of proton transfer is quite sensitive to the quality of PESs and, consequently, to the calculation method used. Thus proton transfer from the enzyme-bound substrate to outer solvent via a series of amino acid residues and the hydroxy group of a coenzyme in liver alcohol dehydrogenase is, according to PM3 semiempirical calculations, a multistage process [47]. Calculations for the same system at SCC-DFTB (Self-Consistent Charge Density Functional Tight-Binding) level predict a concerted mechanism of proton binding [48]. As to experimental studies, we can mention here the work of Yousef et al. [49] who made use of X-ray diffraction data for a 3D crystal structure of an analog of the complex of the transition state for arginine kinase (resolution 1.2 Å) to describe the transition-state structure of the enzyme. These data were considered as evidence for a concerted mechanism of proton transfer in the active site of the enzyme. Of interest are also the experimental results for site-directed mutagenesis in a bacterial reaction center [50], which gave an estimate of 10^5 s^{-1} for the rate of proton transfer over a distance of about 20 Å.

Electrostatic and Donor–Acceptor Interactions on H-bond Proton Transfer

The question on the mechanism of proton transfer in biomolecules is directly related to the question of what properties of hydrogen bond in biomolecules are responsible for the high catalytic activity of the biochemical system. According to suggestions in [51–55], the principal factor responsible for the effectiveness of enzymatic catalysis is formation of short (shorter than 2.5 Å) very strong low-barrier H bonds (LBH bond) in the transition state or in the enzyme–intermediate complex. In terms of this hypothesis, there is a transition from a weak H bond in the enzyme–substrate complex to a strong LBHB in the enzyme–intermediate complex or in the transition state, and the energy gain in the LBHB formation (from 10 to 20 kcal mol^{-1}) facilitates reaction in the enzyme active site.

However, conclusive evidence for existence of strong H-bonds in enzyme active sites is still unavailable, and this question has been vigorously debated since 1990s [56]. In a general case, the strength of an individual H bond in enzymatic catalysis is difficult to estimate. Existence of a strong H bond is frequently established on the basis of geometric and/or spectral criteria. However, as noted in [57, 58], there is no direct evidence showing that the strength of an H bond in the transition state is determined by these experimentally observed properties. An LBHB-stabilized transition state in the active site of an enzyme has never been directly observed experimentally.

The theoretical analysis of the possible catalytic effect of LBHB, performed by Warshel and Papazyan [59], showed that low-barrier H bonds can only exist in nonpolar or low-polarity media where stabilization due to covalent bonding prevails over solvation effects. Thus, the results of EVB calculations for the reaction in the active site of subtisiline (enzyme of the serine protease family) showed that the formation of a tetrahedral intermediate in the active site of the enzyme should occur with a much higher activation barrier than the formation of a LBHB-like configuration in the transition state [59]. The ab initio calculations for model systems in [60], too, revealed no specific stabilization of H-bonded complexes, associated with H-bond shortening, in cases where the pK_a values of the proton donor and proton acceptor are close to each other.

According to an alternative opinion advanced by Warshell and Papazyan [59], the probable reason for

the high catalytic activity of H bonds in the active site of enzymes lies in the fact that reorganization energy, viz. the energy consumed for forming a reactive enzyme–substrate complex, is lower compared with the reaction in solution, on account of a favorable starting arrangement of active groups in the enzyme. Solvating water molecules inside and nearby the active center can play an important role in imparting to the enzyme active center such a polar environment which much better, than water, "solvates" the transitions state [61, 62].

In essence, the LBHB concept explains the catalytic effectiveness of enzymes by donor–acceptor interactions in the "donor–H-acceptor" system, which are characteristic of strong ionic hydrogen bonds. An alternative hypothesis suggests the electrostatic interaction of the transition state with the polar environment of the enzyme active center is the principal stabilization factor.

Simulation of Cooperative Interactions of H Bonds on Proton Transfer

Since proton transfer in biomolecules takes place in a net of H bonds, this process is cooperative in nature. We performed simulation of cooperative interactions in a net of H bonds [63, 64] to establish that parameters measuring donor–accptor and electrostatic interactions in proton-transfer systems correlate with each other. The donor–acceptor interaction are quantitatively measured by the charge Δq transferred between the fragments of the complex and the change in the dipole moment of the complex Δm, which are associated with H-bond proton transfer from the donor to acceptor. An analogous characteristic of the Coulomb interaction is the electrostatic potential of H-bond heteroatoms.

We considered simple ionic molecular complexes with H bonds characteristic of biomolecules, with O, N, and S as proton donors and proton acceptors [63], as well as complexes containing an $FH\cdots F^-$ fragment with a LBHB-like hydrogen bond [64]. Comparative analysis of proton mobility at varied proton positions in neighboring H bonds and configurations of heavy atoms allowed us to reveal a correlation between the electron density distribution in the molecular complex and the electrostatic interaction energy in the donor–prootn–acceptor system and the barrier $E^{\#}$ to proton transfer.

According to ab initio SCF MO LCAO calculations with the 6-31+G** basis set, with inclusion of electron correlation effects at the DFT/B3LYP level, the charge Δq transferred between the fragments of the molecular complex, the dipole moment of the complex, and the difference in the electrostatic potentials $\Delta\varphi = \varphi_D - \varphi_A$ in the transition state of the proton-transfer reaction vary in the same direction (Table 1). As seen from Table 1 which lists the above parameters for the simplest complex $F^1\text{-}H^1\cdots F^{2-}\cdots H^2\text{-}F^3$, the change of the barrier $E^{\#}$ to H^1 transfer in this complex in both directions correlates well with the Δq value for the transition state. This finding suggests that the donor–acceptor interaction plays an important role in proton-transfer processes in H-bonded systems. The strength of the donor–acceptor interaction between the $F–HF^-$ and H–F fragments can also be measured by the energy U_{LUMO} of the lowest unoccupied molecular orbital. As seen from Table 1, the U_{LUMO} in the transition state decreases with increasing Δq.

The fact that the activation barrier to H^1 transfer correlates with the charge transferred to HF is fairly obvious. Decrease of the electron density of the donor decreases its proton affinity, thus facilitating proton transfer to the acceptor (and vice versa). Proton transfer is also favored by increased electron density of the acceptor. According to calculations, the charge Δq transferred between the interacting systems, is a parameter which defines both the change of the dipole moment $\Delta\mu$ of the complex and the potential difference $\Delta\varphi$ between the donor and acceptor.

Dimitrova et al. [65] in their calculations for a series of simple H-bonded molecular systems found a linear correlation between the H-bond energy of the electrostatic potential of the proton. According to our calculations, the barrier to proton transfer correlates with the potential difference $\Delta\varphi$ between the donor and acceptor. Figure 1 plots the calculated barriers $E_i^{\#}$ in the molecular complexes $F^1–H^1\cdots F^{2-}\cdots H^2–F^3$ with varied atomic configurations against the corresponding potential differences $\Delta\varphi_i$ between the donor and acceptor. To include interactions with the polar medium ($\varepsilon = 81$), the SCIPCM solvation model [66] of the self-consistent reactive field theory (SCRF) was used. In agreement with the concept that a polar medium stabilizes, on solvation, structures with a localized charge, the $\Delta\varphi = \varphi_D - \varphi_A$ value increases. However, the planar environment does not alter the character of $E^{\#}$–φ correlation. The effect of solvation

Table 1. Parameters of donor–acceptor and electrostatic interactions on H-bond proton transfer in the $F^1–H^1...F^{2–}...H^2-F^3$ complex[a,b]

$R(F^2...F^3)$, Å	$r(F^2...H^2)$, Å	Δq, au.	δμ, D	$\delta E^{\#}$, kcal mol^{-1}		U_{LUMO}, eV	Δφ, au
				(A→B)	(B→A)		
2.8	1.5	0.125	5.92	19.8	14.3	3.38	0.100
	1.8	0.041	1.42	9.5	7.9	4.43	0.062
3.0	1.4	0.200	9.96	29.1	18.3	2.12	0.158
	1.7	0.097	4.24	15.9	11.9	3.03	0.094
	2.0	0.031	0.15	8.5	6.5	4.41	0.038
3.2	1.6	0.171	7.88	23.4	15.8	1.54	0.105
	1.9	0.075	2.78	12.9	9.6	2.64	0.067
	2.2	0.022	0.0	6.6	5.4	4.33	0.035
3.4	1.5	0.233	11.85	31.1	18.7	0.67	0.137
	1.8	0.128	6.21	19.2	12.8	1.13	0.096
	2.1	0.054	1.49	10.5	7.9	2.16	0.062
	2.4	0.015	0.04	5.5	4.5	4.19	0.033

[a] Parameters for the transition state of the H^1 proton-transfer reaction at a varied position of the H^2 proton of the neighboring H bond: (Δq) negative charge on the $H^2–F^3$ fragment; (δμ) increment of the dipole moment; ($\delta E^{\#}$) change of the proton-transfer barrier; (U_{LUMO}) LUMO energy; and (Δφ), electrostatic potential difference. [b] In states A and B, the H^1 proton resides at F^1 and F^2, respectively.

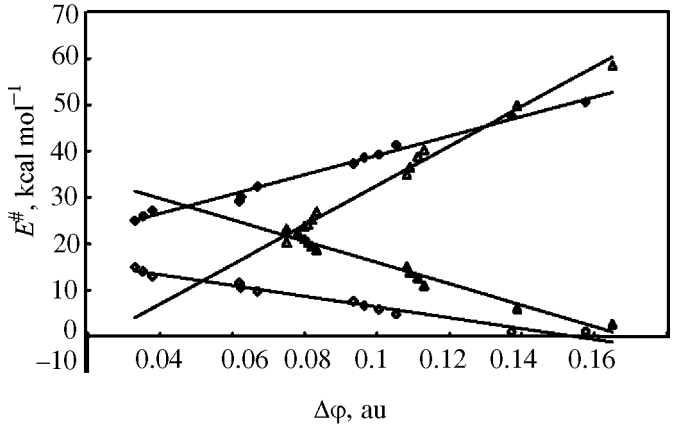

Fig. 1. Plots of the barrier to proton transfer $E^{\#}$ in the $F^1–H^{1...}F^{2-...}H^2–F^3$ complex vs. electrostatic potential difference $\Delta\varphi = \varphi(F^2) - \varphi(F^1)$ between the proton donor and acceptor in the transition state of the reaction: (♦) A → B; (◊) B → A; (D) A → B, SCIPCM; and (▲) B → A, SCIPCM. States A and B are described in the notes for Table 1. (SCIPCM) Calculated with inclusion of solvation effects in terms of the self-consistent reactive field theory.

reveals itself only in changing the slope of the $E^{\#}$–Δφ straight line. The slope is a parameter which relates to the "sensitivity" of the barrier to proton transfer to charge distribution in the molecular complex. The observed correlation between the donor–acceptor and electrostatic interactions explains the linear correlation of the heat of H-bond formation and the increment of the dipole moment of the molecular complex, established experimentally in [67].

Of interest are the results of analysis of the effect on charge distribution and barrier to proton transfer of the length of the quasi-linear H-bond chain that simulates a proton channel [64]. The object for study was linear $(FH)_n\cdots F^-$ clusters, which facilitated analysis of cooperative interactions of H bonds and allowed general quantitative conclusions concerning their role in analogous systems. These clusters were constructed by consecutively adding to the $F–H^1\cdots F^-$ fragment of HF molecules, thus elongating the H-bonded chain with a terminal F^- anion. For each cluster we calculated the total charge on the $F–H^1\cdots F^-$ fragment and the potential curve for H^1 transfer. According to B3LYP/6-31+G** calculations,

Table 2. Effect of H-bond chain length in $(FH)_n^{\cdots}F–H^{1\cdots}F^–$ clusters on charge distribution over chain links and barrier to H^1 proton transfer

n	Δq, au	q_1[a], au	q_2[a], au	$\Delta\varphi$ au	$E^{\#}$, kcal mol^{-1}
			$R(F^{\cdots}F)$ = 2.6 Å		
1	0.052	–0.052	–	0.066	10.8
2	0.069	–0.042	–0.027	0.073	7.8
3	0.075	–0.036	–0.021	0.076	6.9
4	0.077	–0.034	–0.020	0.078	6.6
5	0.078	–0.033	–0.019	0.078	6.4
6	0.078	–0.033	–0.018	0.078	6.3
			$R(F^{\cdots}F)$ = 3.0 Å		
1	0.031	–0.031	–	0.061	12.9
2	0.035	–0.023	–0.012	0.063	11.6
3	0.037	–0.022	–0.010	0.065	11.2
4	0.037	–0.022	–0.009	0.065	11.0
5	0.038	–0.022	–0.008	0.066	10.9
6	0.038	–0.022	–0.008	0.066	10.9

adding each further HF molecule increases the charge Δq transferred from the $F–H^1\cdots F^–$ fragment to links of the H-bond chain and decreases the barrier $E^{\#}$ to the transfer from H^1 to $F^–$ (Table 2). However, the effect of chain length on Δq and $E^{\#}$ gets much weaker as the number of chain links n increases. Therewith, the effect of H-bond chain length is much dependent on the distance R(F···F) between the F atoms in the chain adjacent to the proton donor. Thus, in going from n = 1 to n = 2 at R(F···F) = 2.6 Å, the barrier decreases by 3 kcal mol^{-1}, whereas at R(F···F) = 3.0 Å the decrease is less than 1.5 kcal mol^{-1}. At n > 3, the $E^{\#}$ value is less than 0.5 kcal mol^{-1}, whatever R(F···F).

As to the difference in the electrostatic potentials $\Delta\varphi$ between the donor and acceptor of the H^1 proton, then, as seen from the table, the $\Delta\varphi = \varphi_D - \varphi_A$ value increases with increasing chain length. This increase of $\Delta\varphi$ is associated with the fact that the potential φ_D of F (proton donor) suffers greater changes that φ_A as the number of links in the H-bond chain increases. It is also noted that $\Delta\varphi$ is sensitive to the distance between the HF molecules in the chain. As R(F···F) increases, the "cooperative effect" of the donor–acceptor interaction of hydrogen bonds gets weaker, which prevents charge transfer from $F–H^1\cdots F^–$ and increases $\Delta\varphi$. Thus, at R(F···F) = 3.0 Å, the Δq values at n = 6 proves to be half as high. Further evidence for showing that charge delocalization over chain links gets weaker as R(F···F) increases from 2.6 to 3.0 Å comes from the effective charges q_1 and q_2 on the first and last HF molecules in the H-bond chain.

Proton Transfer in Donor–Chain–Acceptor Systems

Simulation of proton-transfer processes on fairly simple molecular systems showed that water molecules not only effect specific solvation, but also are actively involved in proton exchange. According to calculations for formation and dissociation of quaternary ammonium salts [68], proton transfer by the exchange mechanism involving water molecules which are embedded between donor and acceptor has a much lower activation barrier compared with contact ion pair formation. Another example is the tautomeric transformations of monosuccharides, accompanied by mutarotation. It is well known that succharides in solutions are present as equilibrium mixtures of cyclic and open-chain tautomers. As shown by the calculations in [69], the six-membered ring in glucose should open via proton exchange in water molecules that close the donor–acceptor transfer chain. Comparative analysis of the potential energy surfaces (PES) for molecular systems with H-bond proton transfer showed that exchange reactions feature an earlier transition state that direct doron–acceptor proton transfer.

Translational Mobility of a Bridging Water Molecule and the Mechanism of Proton Transfer (Model of the M_2 Proton Channel of Influenza Virus)

Let us consider the role of water molecules as a mediator in proton-transfer processes in biomolecules using the example of a fairly simple model of the M_2 proton channel of influenza A virus. According to the working hypothesis [70], proton transfer in the M_2 channel occurs via a chain of water molecules that fill the channel. This chain is occluded by the histidine residues of the virus protein coat, which reside roughly

in the center of a bundle of four protein polypeptide helices. The destination of the proton motion is aspartic acid residues at the ends of the polypeptide helices. It is suggested that the histidine residue is directly involved in proton transfer along the M_2 channel [70–72]. First the N_ε-protonated histidine accepts a proton from surrounding water molecules on an unprotonated nitrogen atom of the imidazole ring. A positively charged intermediate with both protonated nitrogen atoms can relax via deprotonation of the N_e center and thus translocate the proton into the water chain. This model is considered to be consistent with the observed proton selectivity of the M_2 channel and pH-dependence of its conductance [70].

In our work on quantum-chemical simulation of the M_2 proton channel we considered a simpler proton-transfer system and focused primarily on the proton transfer via the water chain from the diprotonated histidine to aspartic acid residue [73]. Since the proton affinity of the Asp carboxyl oxygen is higher than that of the imidazole nitrogen, the system with an extra proton localized on the His residue corresponds to a local minimum on the PES, whereas that with protonated Asp residue (endpoint of the proton-transfer chain) corresponds to a global minimum.

In our considered simplest molecular complex methylimidazole–H^+···water···CH_3COO^- than simulated a donor–chain–acceptor chain, hystidine and aspartic acid residues were replaced by protonated methylimidazole and acetate anion, which is a commonly accepted approach in quantum-chemical simulation. In what follows the donor and acceptor groups of the complex are referred to as His and Asp. The water molecule functions as a bridge for imidazole–anion proton transfer (Fig. 2). The N–H^1···O^1 and O^1–H^2···O^2 bond lengths in the complex, calculated by the B3LYP/6-31+G** method with full geometry optimization, show that the water molecule tends to form a shorter and stronger hydrogen bond with the acetate anion. The R(N···O^1) and R(O^1···O^2) distance between the protonated imidazole nitrogen and carboxyl carbon atoms, calculated at R(N···C^1) = 6.5 Å, are 2.849 and 2.645 Å, respectively. Such interatomic distances are typical of H bonds involving nitrogen and oxygen atoms in ionic molecular complexes.

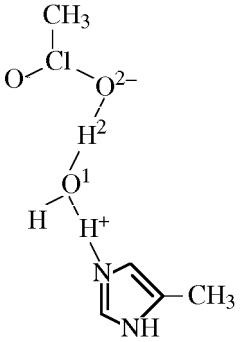

Fig. 2. Molecular complex methylimidazole-H^+···H_2O···CH_3COO^-. The water molecule functions as a bridge for proton transfer from mrthylimidazole to acetate anion.

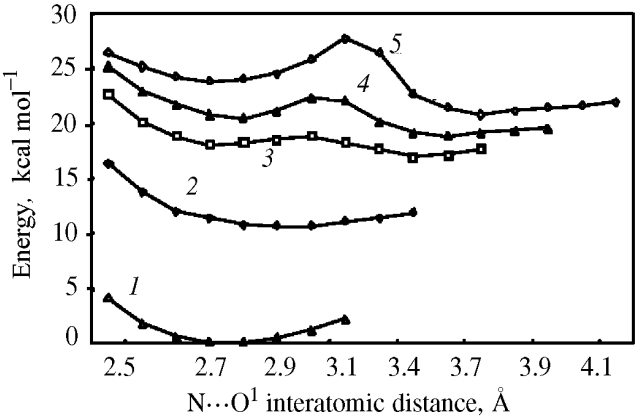

Fig. 3. Change of the total energy of the molecular complex methylimidazole-H^+···H_2O···CH_3COO^- on motion of the water molecule between the proton donor and acceptor at a varied interatomic distance R(N···C^1) (Å): *(1)* 6.5; (*2*) 6.75; (*3*) 7.0; (*4*) 7.25; and (*5*) 7.5. The total energy of the complex at R(N...C^1) = 6.5 Å and an optimized position of the water molecule is taken to be equal to zero.

We were interested in the question: How the distance between the proton donor (His) and proton acceptor (Asp) in the polypeptide helix affects the proton-transfer process? To this end, we performed B3LYP/6-31+G** calculations for the methyl-imidazole–H^+···water···CH^3COO^- complex with varied both R(N···C^1) distance and other geometric parameters. To find out whether the bridging water molecule can freely move between the donor and acceptor, it was successively shifted from imidazole to acetate ion, and, therewith, R(N···C^1) was fixed.

Figure 3 shows the trend of the total energy of the complex on motion of the water molecule for several fixed R(N···C^1) distances. At short His···Asp distances,

Table 3. Atomic charges (after Mulliken), atomic electrostatic potentials, and barriers to proton transfer in the methylimidazole-$H^{+\cdots}H_2O^{\cdots}CH_3COO^-$ molecular complex

$R(N...C^1)$, Å	Effective atomic charge, au				Atomic electrostatic potential, au				$E^{\#,a}$, kcal mol^{-1}
	N(imide)	$O^1(H_2O)$	O^2(Asp)	H^1(imide)	N(imide)	$O^1(H_2O)$	O^2(Asp)	H^1(imide)	
6.5	–0.284	–0.956	–0.676	0.457	–18.205	–22.350	–22.415	–0.902	4.1
6.75	–0.296	–0.860	–0.697	0.457	–18.203	–22.302	–22.424	–0.871	8.9
7.0	–0.343	–0.730	–0.722	0.463	–18.226	–22.220	–22.429	–0.832	18.2
7.25	–0.346	–0.699	–0.726	0.465	–18.232	–22.194	–22.441	–0.815	21.8
7.5	–0.348	–0.686	–0.729	0.466	–18.241	–22.177	–22.452	–0.804	24.7

[a] Barriers to double proton transfer from His to Asp.

the potential curve looks like a well with a flat bottom, i.e. has only one minimum; which implies a fairly free motion of the water molecule. As $R(N\cdots C^1)$ gets longer, the potential curve acquires two wells with a barrier that separates two possible position of the water molecule. The barrier gets higher as the His and Asp residues move away from each other, reaching 4 kcal mol^{-1} at $R(N\cdots C^1)$ = 7.5 Å. It should be noted that the right minimum on the potential curve is lower, which suggests that the water molecule prefers to associate with Asp.

For each of the above-considered configurations of the His$\cdots H_2O\cdots$Asp triad we calculated the potential of proton transfer from His to Asp via the bridging water molecule. At $R(N\cdots C^1)$ = 6.5 Å, the barrier for this double proton transfer is fairly low (ca. 4 kcal mol^{-1}). The position of the water molecule between the donor and acceptor (closer to His or closer to Asp) only slightly affects the height of the barrier. However, as the distance between His and Asp, i.e. $R(N\cdots Cl)$, increases, the barrier to proton transfer becomes to grow (Table 3). As seen from Table 3, this barrier increases to 18 kcal mol^{-1} at $R(N\cdots C^1)$ = 7.0 Å and reaches almost 25 kcal mol^{-1} at при $R(N\cdots C^1)$ = 7.5 Å.

As to mechanistic details of proton transfer, we can mention that in cases where the water molecule can freely move between His and Asp, i.e. at $R(N\cdots C^1)$ < 7.0 Å, both protons move concertedly. Vice versa, when the water molecule has to overcome barrier on its motion, the energetically most probable mechanism involves successive motion of two protons.

Table 3 lists the effective charges on the O and N atoms that function as the proton donor and acceptor, as well as the bridging hydrogen H^1 which is transferred to the water molecule at the initial stage of the process. i.e. when His still bears a positive charge. As the distance between His and Asp, as well as the barrier to proton transfer increases, a clearly defined tendency for an increase of the negative charge on N and O^2 and a decrease of the negative charge on the intervening O^1 atom of the water molecule.

As to the electrostatic potentials of the same atoms, they vary in parallel to the atomic charges (Table 3). Figure 4 presents the plots of the barriers to proton transfer versus the potential differences Δφ between N and O^1. The observed correlation between $E^{\#}$ and Δφ is consistent with the results of calculations for simple H-bonded molecular complexes. Note that the

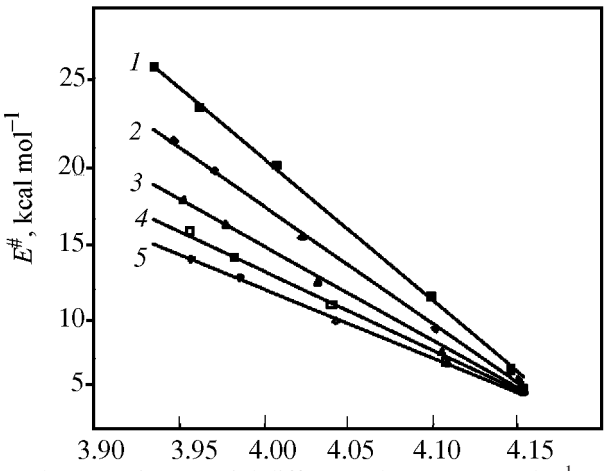

Fig. 4. Effect of the number of water molecules in the H-bonded chain and the donor–acceptor distance on the barrier to proton transfer in the complex methylimidazole-$H^+...(H_2O)_n...CH_3COO^-$. Figures above the plots relate to the number of water molecules in the chain bridging protonated imidazole and CH_3COO^- anion.

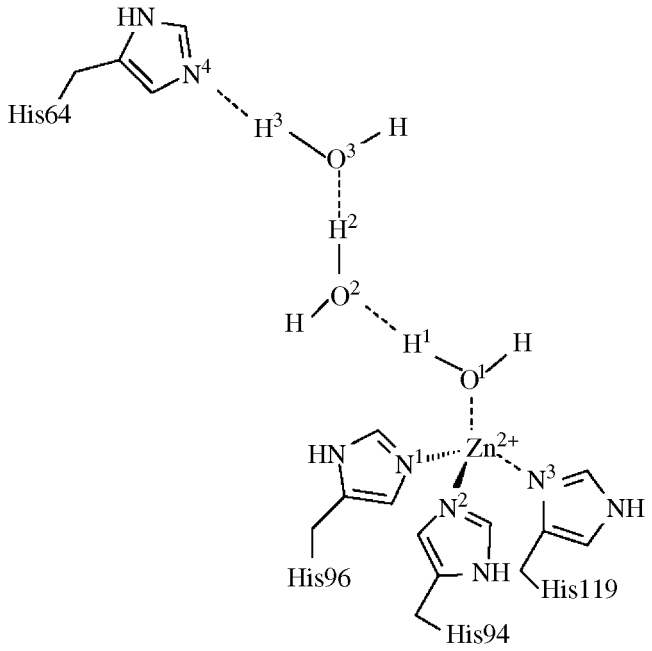

Fig. 5. Structure of the complex simulating the proton channel in the active site of carboanhydrase II.

increase of the negative charge on O^1 makes it easier for proton to move in its direction. Therefore, as $\Delta\varphi$ increases with increasing potential of oxygen, the barrier to proton transfer in this direction decreases. As seen from Fig. 4, the linear correlation between $E^{\#}$ and $\Delta\varphi$ is preserved whatever the number of bridging water molecules. Such chains were constructed by increasing the $R(N\cdots C^1)$ distance by 2.5 Å with every added bridging water molecule, followed by geometry optimization of the complex. As the chain is elongated, the sensitivity of barrier to transfer to potential difference (slope of the straight line) decreases. The slope k of the equation $E^{\#} = k\Delta\varphi + b$ has the dimension of charge, and it can be considered as a measure of charge transfer, i.e. proton charge. Actually, k is roughly equal to 0.5, which is fairly close to the charge on the transferred proton (Table 3).

Proton-Transfer System of the Active Site of the Enzyme Carboanhydrase

Another interesting proton donor–chain–acceptor molecular system is a proton-transfer molecular complex of the active site of the enzyme carboanhydrase. Carboanhydrase is an exceptionally effective catalyst of reversible CO_2 hydrolysis, which comprises 250 amino acid residues and a Zn cofactor [74]. The mechanism of this enzyme catalysis has been the subject of vigorous experimental [75–81] and theoretical [61, 82–91] research over the past decades. A number of genetically and immunologically different but structurally homologous carboanhydrase isozymes are known, which have different kinetic characteristics and ligand-binding abilities. Nevertheless, the catalytic mechanisms are probably common for all forms of this enzyme. Studying the mechanism of catalysis of CO_2 hydration on the enzyme active site proved very useful for understanding features of proton transfer in enzyme systems.

The catalytic mechanism involves two stages. The first is the conversion of CO_2 into HCO_3^- [reaction (1)], as a result of direct nucleophilic attack on CO_2 of the hydroxy group bound with Zn [77, 80]. The second stage involves proton transfer, as a result of which the hydroxyl is regenerated [reaction (2)].

$$CO_2 + EZnOH^- + H^2O \rightleftharpoons HCO_3^- + EZnH_2O \quad (1)$$

$$\text{His64-EZnH}^2\text{O} + B \rightleftharpoons H^+\text{His64-EZnOH}^- + B \rightleftharpoons \text{His64-EZnOH}^- + BH^+, \quad (2)$$

B is buffer and His-64 is the amino acid residue which accepts proton in carboanhydrase (CA II).

Until now there has been no clear understanding of the mechanism of proton transfer in the active site of carboanhydrase. Silverman and Lindskog [77] in their comprehensive experimental research obtained evidence for the suggestion of Steiner et al. [75] that the proton transfer between the Wat1 molecule bound with Zn^{2+} and the His-64 residue in CA II is intermolecular. Since the distance between His-64 and Wat1 is too large for direct proton transfer to be possible, this process should develop via a chain of built-in water molecules contained in the crystal structure of the enzyme and forming a net of H bonds [92, 93]. It is suggested that the mechanism of proton translocation is similar to that of proton transfer over a chain of water molecules that form the proton channel in gramicidin [94]. The structure of the molecular complex that simulates the proton-transfer system in CA II is shown in Fig. 5.

According to the resulting data, the pK_a of Wat1 (~7) is almost the same as that of the protonated His-64 residue. Close pK_a values are important for mutual proton exchange, since different pK_a values can entail

Table 4. Interatomic distances (*R,* Å) in the model proton-transfer complex of the active site of carboanhydrase II[a, b]

R	IS	FS	TS_1	TS_2
$O^1 \cdots O^2$	2.495(2.530)	2.666(2.575)	2.499(2.447)	2.423
$O^2 \cdots O^3$	2.574(2.539)	2.643(2.687)	2.372(2.379)	2.427
$O^3 \cdots N^4$	2.783(2.755)	2.616(2.627)	2.660(2.649)	2.507
O^1–H^1	1.010(1.003)	1.696(1.596)	1.483(1.305)	1.053
O^2–H^1	1.486(1.546)	0.973(0.994)	1.018(1.052)	1.370
O^2–H^2	0.986(1.004)	1.670(1.713)	1.129(1.131)	1.065
O^3–H^2	1.588(1.535)	0.974(0.977)	1.243(1.249)	1.362
O^3–H^3	0.975(0.988)	1.560(1.576)	1.001(1.014)	1.290
N^4–H^3	1.809(1.770)	1.056(1.061)	1.659(1.636)	1.217
Zn–O^1	1.965(1.983)	1.860(1.872)	1.892(1.901)	1.943
Zn–N^1	2.092(2.077)	2.128(2.114)	2.123(2.114)	2.094
Zn–N^2	2.091(2.097)	2.116(2.124)	2.111(2.119)	2.095
Zn–N^3	2.091(2.097)	2.116(2.124)	2.111(2.119)	2.095
$Zn \cdots N^4$	8.662(7.679)	8.896(8.162)	8.538(7.901)	8.258

[a] (IS, FS) Initial and final states of the complex, respectively; (TS_1, TS_2) possible transition states of the proton-transfer reaction. Ab initio calculations with the 6-311G (6-31G) basis set. [b] (N^1, N^2, N^3) Imiodazole nitrogens coordinated to Zn^+ (see Fig. 5).

a considerable barrier to proton transfer in one or the other direction. In fact, this requirement excludes other functional groups or amino acid residues from proton transfer [85]. The results of Qian et al. [81] for isozymes CA III (Lys-64) and CA V (Tyr-64) gave evidence for the proposed mechanism of proton transfer. Experiments on site-directed mutagenesis showed that in both cases the number of enzyme turnovers in the catalytic cycle can be increased by replacement of the amino acid residue in the 64 position by histidine. Moreover, it was found that the maximum catalysis rate is increased by replacement of Lys-64 and Tyr-64 by glutamate and aspartate which can provide effective proton transfer at pH = 6–8.

According to X-ray diffraction data [95], the Zn^{2+} ion in CA II is at a distance of 7.8 Å from His-64, which allows for at least three water molecules to built-in between them to form a "bridge" for proton transfer (see Fig. 5). The imidazole ring in His-64 can function according to Eq. (2), by providing proton transfer from the active site of the enzyme into the buffer solution. Experiments on hydrogen isotope exchange in solvent and measurements of the rates of transition of ^{18}O-labeled water molecules in solvent with varied contents of buffer solution [76] showed that proton transfer between Wat1 and His64 is a stage that limits the catalysis rate at a high content of buffer solution, whereas the limiting stage at low contents of buffer solution is proton transfer to the medium.

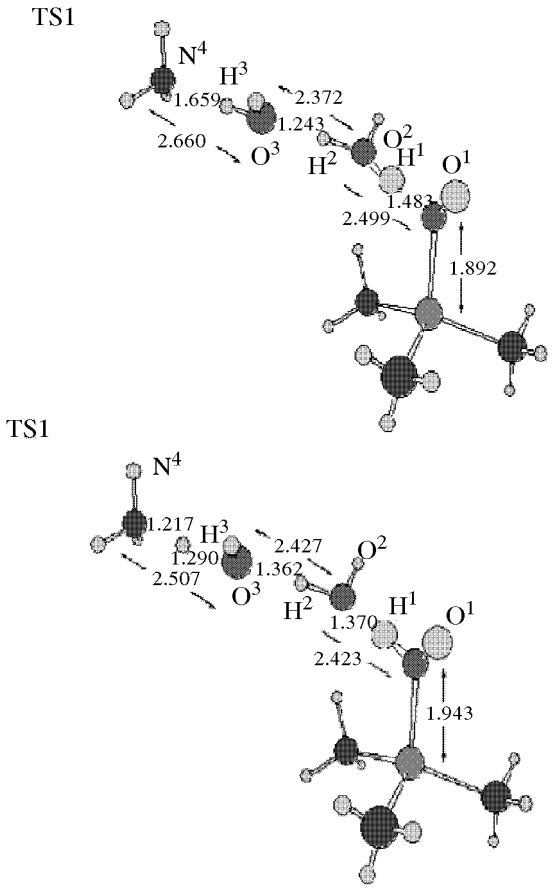

Fig. 6. Structures of the transition states TS_1 and TS_2 in the proton-transfer reaction in the molecular complex $(NH_3)_3Zn^{2+} \cdots OH_2 \cdots OH_2 \cdots OH_2 \cdots NH_3$.HF/6-311G calculations.

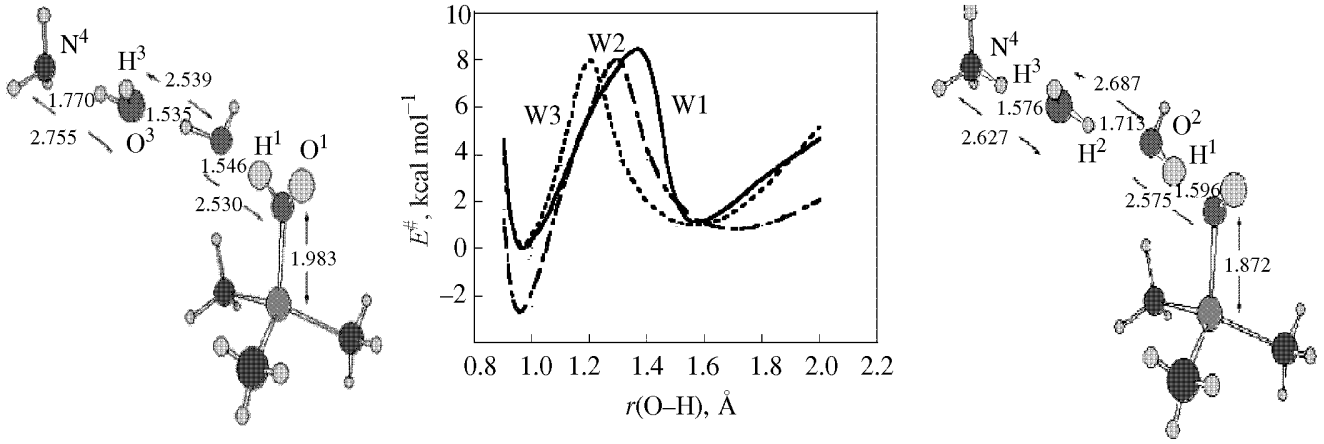

Initial equilibrium complex

Proton-transfer product

Fig. 7. Potential curves of proton transfer in the molecular complex $(NH_3)_3Zn^{2+}\cdots OH_2\cdots OH_2\cdots OH_2\cdots NH_3$. Curve W1 relates to the case when the process is initiated by a shift of the first water proton, and curves W2 and W3 were obtained using as "engines" the second and third water protons, respectively. HF/6-31G calculations [98].

To assess the barrier to proton transfer from zinc to histidine in carboanhydrase (hydration reaction), a variety of model systems and theoretical methods have been used. However, this was either semiempirical calculations or calculations with "bad" basises [61, 82, 83] or calculations involving no geometry optimization [88], i.e. calculations of not quite realistic models, since the water molecules in the enzyme active site possess translational and vibrational mobility. The measured kinetic isotope effects [96, 97] gave evidence to show that more than one proton can be involved in the transition state and, consequently, proton transfer can be associated with motion of both donor and acceptor. We performed ab initio calculations [98, 99] of the molecular complex simulating the proton-transfer system in the active site of CA II, with allowance for the mobility of all water hydrogen and oxygen atoms that form the proton-transfer channel. The geometric and electronic structures of the transition state of the proton-transfer reaction in the active site of CA II were also calculated.

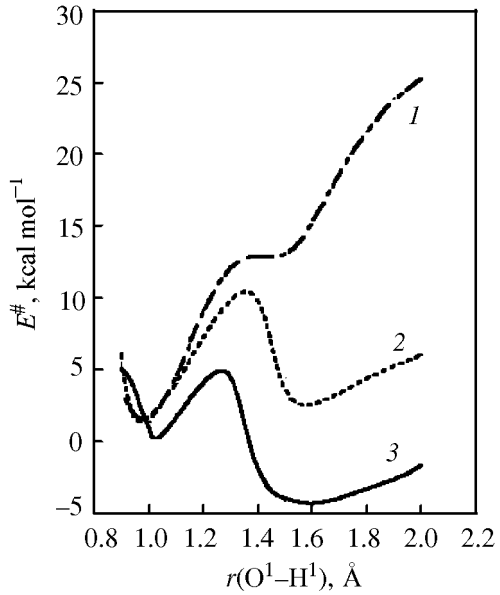

Fig. 8. Potential curves of proton transfer in the molecular complex $(NH_3)_3Zn^{2+}\cdots OH_2\cdots OH_2\cdots OH_2\cdots NH_3$, obtained at varied constraints on the geometry of the complex: *(1)* H^1 motion at a fixed positions of water molecules in the proton channel; (*2*) H^1 motion at fixed distances between Zn^{2+} and ligands: R(Zn–O) = 2,0 Å, R(Zn–N) = 2.1 Å (see Fig. 7); and (*3*) calculation with full geometry optimization of the complex.

In constructing an appropriate model whose size allows fairly accurate ab initio calculations we replaced histidine residues (see Fig. 5) by ammonia molecules (such replacement of the imidazole ligands is commonly accepted in theoretical studies on biochemical systems [100]). Binding centers of a transition metal in protein generally contain 3–4 amino acid ligands. The Zn^{2+} ion in carboanhydrase coordinates three hystidine residues. Importantly, these ligands have no side hydrogen atoms and, consequently, are unable to form H bonds with bridging water molecules.

The equilibrium geometries of the molecular complex $(NH_3)_3Zn^{2+}\cdots OH_2\cdots OH_2\cdots OH_2\cdots NH_3$, which

corresponds to the initial state of the system with the water molecule at Zn^{2+} and to the final state formed by proton transfer to ammonia, as well as to two possible transition states, as given by our HF/6-31G and HF/6-311G calculations [98, 99], are presented in Table 4. As seen, calculations with both basis sets predict close H-bond lengths in the proton-transfer channel. Even though the water–water H bonds are very short, water protons are clearly associated with donor atoms.

The calculated Zn^{2+}–ligand distances R(Zn–N) for the initial state of the system vary from 2.08 to 2.10 Å, and the distance between Zn^{2+} and the water molecule R(Zn–O) is slightly shorter (1.97–1.98 Å). These values are close to those obtained by other methods. Thus, the following values for the initial state were obtained by X-ray diffraction: R(Zn–N) = 2.1–2.3 Å, R(Zn–O) = 1.9–2.0 Å [101, 102]. Molecular mechanics calculations for solvated carboanhydrase CA I predict that Zn^{2+} has a slightly distorted tetrahedral coordination: 1.936 Å < R(Zn–N) < 1.974 Å and R(Zn–O) = 1.923 Å [84]. According to molecular dynamics simulation with ab initio bond parameters for ligands, the mean distance between Zn^{2+} and His residues is 2.10–2.15 Å [87].

Table 5. Barriers to proton transfer (kcal/mol) calculated for the $(NH_3)_3Zn^{2+}\cdot\cdot OH_2\cdot\cdot OH_2\cdot\cdot OH_2\cdot\cdot NH_3$ complex at different levels of theory

Calculation method	$E^{\#}$	$E^{\#}$ + ZPVE[a]
SCF		
HF/6-31G	5.3	1.0
HF/6-31G*//HF/6-31G	10.7	6.5
HF/6-31G**//HF/6-31G	8.5	4.3
HF/6-31+G**//HF/6-31G	8.6	4.4
post-SCF		
B3LYP/6-31+G**// HF/6-31G	2.3	0.0
MP2/6-31+G**//HF/6-31G	3.4	0.0

[a] The barrier to proton transfer is corrected for zero-point vibration energy.

Table 6. Lengths of hydrogen bonds in the $(NH_3)_3Zn^{2+\cdots}(H_2O)_n{}^{\cdots}NH_3$ molecular complex[a]

Calculation method	Number of links, n	$O^{1\cdots}O^2$	$O^{2\cdots}O^3$	$O^{3\cdots}O^4$	$O^{4\cdots}O^5$	$O^{5\cdots}O^6$	$O^{6\cdots}O^7$	$O^{7\cdots}O^8$	$O^{8\cdots}O^9$	$O^{9\cdots}O^{10}$	$O^{10\cdots}O^{11}$	$O^{11\cdots}N$
HF/6-31G	4	2.524	2.523	2.585	2.788							
	5	2.558	2.664	2.540	2.597	2.793						
	6	2.517	2.718	2.697	2.549	2.601	2.797					
	7	2.639	2.656	2.799	2.743	2.530	2.597	2.795				
	8	2.643	2.658	2.798	2.737	2.519	2.582	2.623	2.812			
	9	2.641	2.657	2.766	2.892	2.587	2.771	2.563	2.615	2.808		
	10	2.641	2.655	2.763	2.892	2.586	2.769	2.552	2.598	2.634	2.820	
	11	2.646	2.591	2.853	2.833	2.589	2.752	2.744	2.550	2.599	2.634	2.819
B3LYP/6-31+G**	6	2.679	2.724	2.798	2.757	2.540	2.702					
	11	2.803	2.644	2.805	2.735	2.662	2.823	2.765	2.574	2.615	2.650	2.777

[a] The atoms are numbered from donor to acceptor (from Zn^{2+} along the chain).

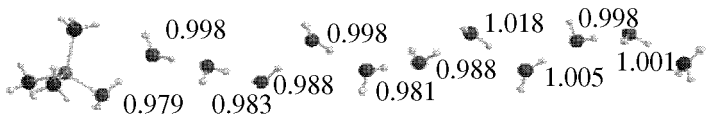

Fig. 9. Distribution of O—H bond lengths (Å) along the water chain in the molecular complex $(NH_3)_3Zn^{2+}\cdots(H_2O)_{11}\cdots NH_3$. B3LYP/6-31+G**calculations.

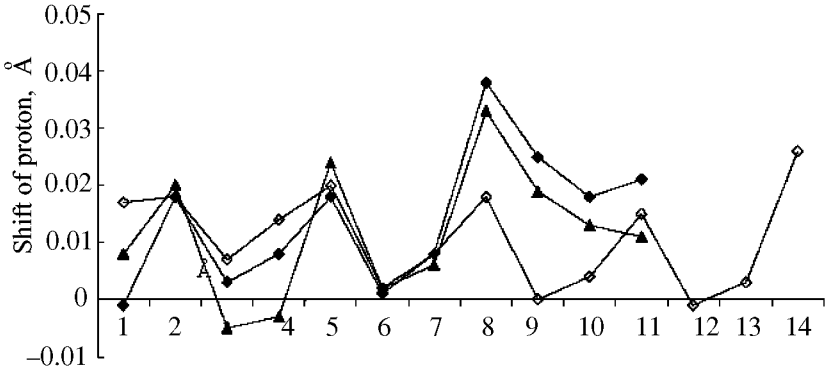

Fig. 10. Shifts of H-bond protons in the complexes $(NH_3)_3Zn^{2+}...(H_2O)_{11}...NH_3$ (C_{11}) and methylimidazole$(H^+)\cdots(H_2O)_{14}\cdots CH_3COO^-$ (I_{14}) complexes with respect to their equilibrium positions in an isolated water chain: (▲) C_{11}(HF/6-31G); (♦) C_{11}; and (◊) I_{14}. B3LYP/6-31+G** calculations. The chain links are numbered from Zn^{2+} to the final acceptor NH_3 in complex C_{11} and from the imidazole to anion in complex I_{14}

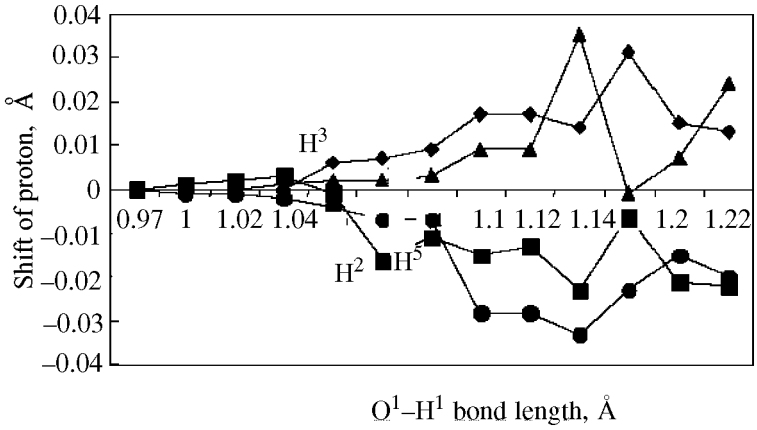

Fig. 11. Shifts of the second–fifth chain link protons (H^2, H^3, H^4, H^5) with respect to their equilibrium positions in the complex $(NH_3)_3Zn^{2+}...(H_2O)_{11}...NH_3$ (C_{11}), with increasing O^1–H^1 distance.

The fact that there are short H bonds in the proton channel suggests that the barrier to proton transfer over them is fairly low. According to our calculations [99], the proton-transfer reaction IS→FS can occur via structurally different transition states, depending on what proton (H^1, H^2, or H^3) initiates the process. Figure 6 shows what changes occur in the structure of the transition state when the reaction-controlling proton changes from H^1 to H^3 (see also Table 4). As the O^1–H^1 bond gets longer as H^1 is moving along the axis of the H bond between O^1 and O^2, the reaction occurs via TS_1. In this case, the proton common for two first water molecules in the chain is used as an "engine" that controls the process. In the calculations,

Table 7. Charges on water molecules in the H-bond chain on H^1 proton transfer in the $(NH_3)_3Zn^{2+}...(H_2O)_{11}...NH_3$ (C_{11}) complex

O^1–H^1 bond length, Å	Charge on water molecules[a], e										
	1	2	3	4	5	6	7	8	9	10	11
0.972[b]	0.060	0.036	0.001	0.010	0.029	0.016	0.015	0.024	0.013	0.008	0.004
1.10	0.056	0.042	0.016	0.013	0.027	0.010	0.013	0.024	0.013	0.007	0.004
1.14	0.057	0.059	0.041	0.017	0.010	0.025	0.009	0.021	0.011	0.006	0.003
1.18	0.043	0.071	0.039	0.0	0.008	0.026	0.013	0.016	0.025	0.011	0.005
1.22	0.015	0.084	0.027	0.037	0.009	0.012	0.028	0.012	0.009	0.020	0.005

[a] The numbers **1**–**11** relate to the chain link number. [b] The O^1–H^1 bond length of 0.972 Å corresponds to the equilibrium geometry of the $(NH_3)_3Zn^{2+}\cdots(H_2O)_{11}\cdots NH_3$ complex.

the $r(O^1\cdots H^1)$ distance was increased in 0.1-Å increments, and, at each fixed position of H^1, positions of the two other protons H^2 and H^3 were optimized. The calculated proton-transfer potential curves are presented in Fig. 7 (curve W1). The corresponding proton-transfer barrier is 8–9 kcal mol^{-1}. According to calculations, as H^1 moves, the other two protons, too, move from the donor to acceptor, and such a motion of all the three protons along the H-bond chain can be defined as a "concerted" process.

Note close barriers to proton transfer in all the three cases presented by the curves W1, W2, and W3 in Fig. 7. The latter two curves were obtained with H^2 and H^3 as engines. Thus, the potential curve W3 corresponds to the motion of H^3 along the H-bond axis at a step of 0.1 Å, the positions of H^1 and H^2 being optimized. If the IS□FS process occurs via H^3 proton transfer (elongation of the O^3–H^3 bond), then the transition state is TS_2 (see Fig. 6 and Table 4).

Even though the barrier to proton transfer is independent of what proton controls the process (the downward shift of the left minimum on the W2 curve reflects a geometric feature of the complex at $r(O^2\cdots H^2)$ = 0.95 Å); the potential curves in Fig. 7 are not identical, since their maxima relate structurally different transition states. The barrier shifts to the left in going from W1 to W2, and further to W3, and, therewith, the potential curve gets narrower.

The most important factor that affects the proton-transfer barrier is translational mobility of water molecules along the proton channel. The proton-transfer potential curve at fixed positions of heavy atoms (rigid geometry of the proton channel) has only one minimum (Fig. 8, curve *1*). The relaxation of

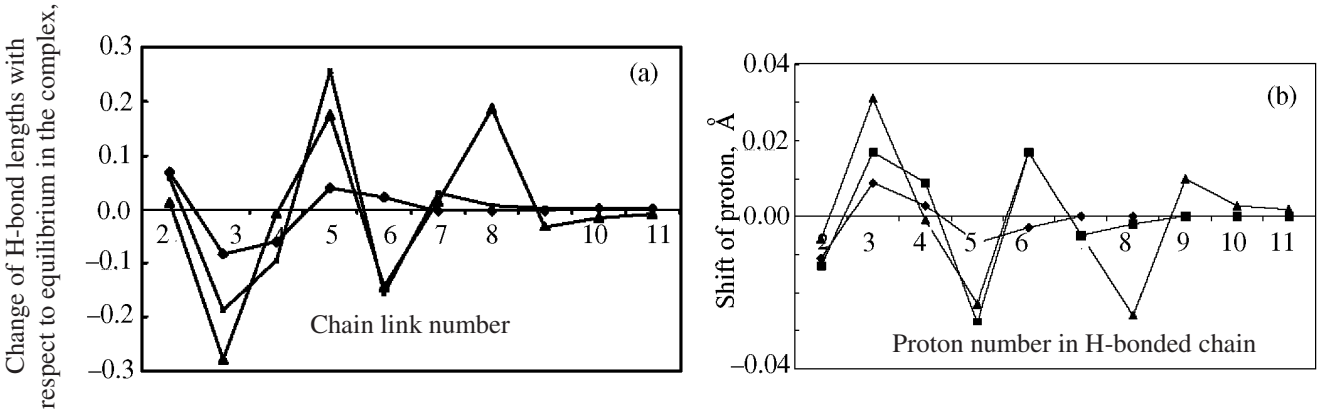

Fig. 12. (a) Propagation of H-bond deformation wave, associated with H^1 motion, along the water chain from the donor (Zn^{2+}) to acceptor in the complex $(NH_3)_3Zn^{2+}\cdots(H_2O)_{11}\cdots NH_3$ and (b) fluctuations of O–H bond lengths on H^1 transfer. $r(O^1$–$H^1)$, Å: (♦) 1.10; (■) 1.14; and (▲) 1.18.

Zn^{2+}–ligand bond lengths on proton transfer strongly affects the transfer barrier and the relative stability of the initial structure and the transfer product. Calculations with optimization of Zn^{2+}–ligand distances predict the decrease of the barrier to 5 kcal mol^{-1} and an exothermic process.

As seen from data in Table 5, the calculated barrier to proton transfer depends on what is the size of the basis set and whether electron correlation effects or zero-point energy are included. When the basis is extended to include polarization functions of heavy atoms (*), the barrier tends to increase. Vice versa, polarization functions on H atoms (**) and diffuse functions on heavy atoms (+) decrease the barrier. The decrease of the energy barrier, that occurs on inclusion of electron correlation, much bypasses all changes produced by basis set extension. The zero0point vibration energy is about 4 kcal mol^{-1}. According to the estimates of Lu and Voth [88], replacement of the model NH_3 molecules by imidazole molecules increases the barrier by about 15 kcal mol^{-1}. Taking account of the fact that different effects, such as basis set extension, inclusion of correlation, and transfer to amino acid residues in simulating the ligands, have opposite effects on the barrier to proton transfer, we can conclude that the calculated barrier is close to known experimental estimates (10–15 kcal mol^{-1}).

Quantum-chemical calculations [91] for an extended molecular system containing imidazole molecules as hystidine residues, with electron correlation effects included at the B3LYP level of theory, gave evidence for our suggestion [98] that the proton transfer over the chain of H bonds occurs by a concerted mechanism, as well as for estimates of the barrier. Smedarhina et al. [103] performed direct dynamic calculations for the proton-transfer process, rate constants and kinetic isotope effects for a model system comprising 58 atoms and including a four-cordinate zinc ion bound with the methylimidazole molecule by a chain of water molecules. The results of these calculations, too, suggest a concerted mechanism of proton transfer in the active site of the enzyme.

Wave Mechanism of Proton Transfer over an H-Bond Chain Linking Donor and Acceptor

Exact number and positions of water molecules in the chain between Zn^{2+} with the acceptor His-64 in the active site of carboanhydrase are impossible to determine by experiment. Thus, Toba et al. [89] in their molecular dynamics simulation of the active site of carboanhydrase in the aqueous phase revealed the possibility of formation of a stable bridge comprising three to seven water molecules. The question of how the number of water molecules in the proton channel affects the mechanism and barrier to proton transfer is still poorly studied. To establish parameters of an H-bond chain which might function as an effective proton conductor, we considered the complexes $(NH_3)_3Zn^{2+}\cdots(H_2O)_n\cdots NH_3$ (hereinafter labeled C_n) with a varied number of water molecules n in the H-bond chain [73, 104].

Table 6 lists the O···O H-bond lengths obtained by calculations for complexes C_n ($4 < n < 11$) with their geometry optimization. In complex C_{11} with the longest chain ($n = 11$), there is clearly defined alternation in H-bond lengths along the chain; therewith, the shortest H bonds are realized between the second and third, fifth and sixth, as well as eighth and ninth water molecules. The H bonds are shorter by 0.2 Å compared with the equilibrium H-bond length in an isolated chain of water molecules. The observed pattern corresponds to a periodicity of three chain links. It should be emphasized that the same distribution of H-bond lengths was obtained by HF and DFT/B3LYP calculations.

In shorter chains, the positions of H-bond contraction maxima are different. Thus, in the complex comprising a chain of five water molecules (complex C_5), the shortest H bonds are between the first and second, as well as third and fourth water molecules.

Therewith, there are certain regular trends in variation of the positions of maxima with the number of chain links. In going from C_5 to C_{11}, first the second contraction maximum shifts along the chain toward the acceptor, whereas the first maximum preserved its position. Then, at $n = 9$, the third maximum appears which, too, tends to shift. In an 11-link chain, the three H-bond contraction maxima are equidistant from each other. The variation of O–H bond lengths in the H-bonded chain reflects periodicity in H-bond lengths (Fig. 9).

Figure 10 shows the shifts of H-bond protons in complex C_{11} with respect to their equilibrium positions in an $(H_2O)_n$ chain with lacking $(NH_3)_3Zn^{2+}$ donor and NH^3 acceptor. In other words, the shifts in complex C_{11} are defined by the effects of the above groups on

O–H bond lengths in the chain. As would be expected, the trend in variation of O–H bond lengths along the chain is opposite to that for H-bond lengths, i.e. O–H elongation maxima coincide with H-bond contraction maxima. Since the shortest O···O distances in complex C_{11} are observed for the 2–3, 5–6, and 8–9 links, the largest elongation of O–H bonds takes place in the second, fifth, and eighth water molecules. The vibration amplitude of O–H bond length along the chain is 0.02–0.04 Å, and it slightly increases as the maximum shifts away from the Zn^{2+} ion. As seen from Fig. 10, HF/6-31G and B3LYP/6-31+G** calculations predict an almost identical shape of "proton wave".

Figure 10 presents similar data for the molecular complex methylimidazole $(H^+)\cdots(H_2O)_{14}\cdots CH_3COO^-$ (I_{14}) containing 14 water molecules, which allows comparisons with complex C_{11}. Even though the water chains have different lengths, and the donor and acceptor end groups are different, the distributions of O–H bond lengths along the water chain in both systems are similar: The positions of maxima in the "proton wave" almost coincide, and the amplitudes are quite close to each other. The distance between neighboring maxima on the "proton wave" (H-bond contraction maxima), which can be defined as bond length, is about 8 Å.

In the preceding section we considered equilibrium structural features of water chains. Of no less interest is H-bond proton motion between oxygen atoms along the chain and degree of synchronization of the motion of different protons. To gain insight into these problems, the proton H^1 that belongs to the first link of the water chain was consistently shifted along the $O^1\cdots O^2$ chain. At each H^1 position, positions of other H-bond protons were optimized. In these calculations, we set constant the distance between the zinc ion and ligand nitrogen atoms (2.1 Å) and O^1 (2.0 Å). Figure 11 shows how the position of H^1 on the $O^1\cdots O^2$ H-bond line affects the positions of the following four chain protons in complex C_{11}. As H^1 shifts toward O^2, the following proton H^2 first moves away from the oxygen atom, and the O^2–H^2 bond gets slightly longer. However, on further H^1 transfer this tendency is reversed, and H^2 moves back to O^2. Interestingly, the H^2 and H^5 protons in H-bond contraction maxima shift in a counter phase with respect to H^3 and H^4. For example, when H^2 and H^5 get closer to the donor oxygen atoms, H^3 and H^4 move away from each other. As a result, the contraction of O–H bonds in the first case corresponds to their elongation in the second. The motion of all the four protons can be defined as vibrational, since they move forward and back during H^1 proton transfer from O^1 to O^2.

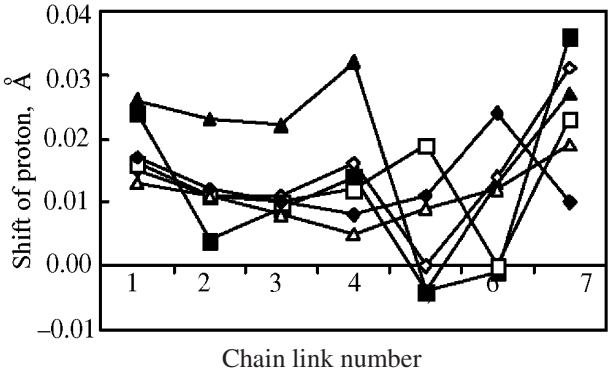

Fig. 13. Dependence of the central maximum position on *R* ($N^{\cdots}C^1$) in the complex methylimidazole $(H^+)\cdots(H_2O)_7\cdots CH_3COO^-$ (according to B3LYP/6-31+G** calculations, see Fig. 2). *R* ($N^{\cdots}C^1$), : Å: (■) optimization; (▲) 15; (◊) 17; (□) 19; (♦) 21; and (Δ) 23.

The "proton waves" presented in Fig.12 allow us to trace dynamics for all chain links during H1 motion in complex C_{11}. The trend in O···O distances, associated with the first proton motion from O^1 to O^2, is shown in Fig. 12a. Elongations and contractions reflect what can be described as the deformation wave. For example, the third link in the chain is the most contracted irrespective of how far H^1 has shifted. This contraction enhances as the O^1–H^1 distance increases to 1.10 Å and then to 1.14 and 1.18 Å. Analogously, the elongation observed in the fifth link corresponds the strongest increase of the O···O distance in the chain. At the same time, the response of the fourth link on H^1 shift is very weak. Consequently, the 3th and 5th links are peaks on the wave, separated by the node at the 4th link. As seen from Fig. 12a, there is one more node at the 7th link.

Figure 12b shows changes in O–H bond lengths, corresponding to changes in H-bond lengths. Here, too, we can see a wave with nodes at the 4th and 7th links; this wave is dissymmetrical to that Fig. 12a. The waves in Figs. 12a and 12b are likely to propagate until the 9th link, and further on the effect of H^1 shift is appreciably attenuated. Note that as H^1 shifts from 1.10 to 1.14 Å, and further to 1.18 Å, the deformation wave propagates along the chain. Additional calculations (not given here) show that the wave begins to shift to the right

at $r(O^1–H^1) > 1{,}18$ Å and propagates until all protons completely shift from the donor to acceptor. At $r(O^1–H^1) = 1.22$ Å the wave reaches the right end of the H-bonded chain, and even H^{11} appreciably shifts toward the NH_3 acceptor.

Another aspect of the periodicity in the H-bonded chain follows from an analysis of the electron density distribution in molecular complex C_{11}. The data in Table 7 show the changes in the charges on water molecules in complex C_{11}, associated with proton displacements along the chain. As seen, the charge on certain water molecules, say 1st, 5th, and 8th, gradually decreases during the proton-transfer process, and whereas the charge on the other molecules grows. The charge of certain molecules fluctuates; for example, the charge on the third molecule first increases and then decreases. One more evidence for the fluctuating behavior of the molecular charges comes from the data for the 7th molecule whose charge reaches a minimum in the middle of the proton-transfer process.

The wave analogy can be developed further. If the proton wave frequency is taken to be equal to the frequencies of O–H bond vibrations that initiate the wave, then the wave number of about 3000 cm^{-1} will correspond to the frequency of 9×10^{13} s^{-1}. Since the length of the proton wave is about 8 Å, then, in view of the above-mentioned frequency, the wave velocity should be 7×10^4 m s^{-1}. Taking the whole distance for the wave to propagate equal to the length of the H-bond chain between the donor and acceptor (30 Å), the time of this process can be estimated at 4×10^{-14} s = 40 fs. Note that this estimate is close to those for the proton transfer in aromatic Schiff bases, obtained by means of femtosecond spectroscopy [105].

It is interesting to consider how the donor–acceptor distance affects H-bond proton positions. To this end, we have studied complex I_7 in which the protonated methylimidazole and $CH^3COO^–$ are intervened by a chain comprising seven water molecules [73]. In our calculations for this complex at varied fixed interatomic distances $R(N\cdots C^1)$ (see Fig. 2) and optimization of other geometric parameters we determined the shifts of H-bond protons relative to their positions in the same complex but in the absence of protonated methylimidazole and $CH^3COO^–$ anion (Fig. 13). When $R(N\cdots C^1)$ is equal to or smaller than 17 Å, we observe an appreciable proton shift in the middle-chain 4th link. However, as the donor–acceptor distance increases, the maximum shift is already observed in the fifth link at R = 19 Å, and then in the sixth link at R = 21 Å, and, finally, in the last, seventh link at R = 23 Å. In the last case, the minimal proton shift is observed in the middle of the chain, i.e. the O–H bond in the 4 water molecule proves to be the shrtest in the chain.

CONCLUSIONS

Our research showed that the barrier to proton transfer in a complex in which the proton donor and proton acceptor are bridged by a water molecule is independent of the position of the bridging molecule. However, the energy barrier tends to increase with increasing distance between the donor and acceptor. Double proton transfer occurs by a concerted mechanism, if the potential that describes the translational motion of water molecules have a single minimum; in the case of a two-well potential, successive proton transfer takes place. As the number of water molecules in the chain increases, the barrier to proton transfer, which is linearly related to the difference in the electrostatic potentials between the donor and acceptor, becomes less sensitive to donor–acceptor distance.

The lengths of H and O–H bonds were found to fluctuate as proton shifts along the water chain bridging the donor and acceptor. Proton transfer is associated with propagation of H-bond deformation wave along the chain. As the wave propagates along the chain, which can be referred to as vibrational motion of separate H-bond protons, the electron charge is transferred from one end of the chain to the other. The wave length is about three chain links. Provided the wave frequency is equal to O–H vibration frequency, the wave velocity can be estimated at about 7×10^4 m s^{-1}, and the time of proton transfer along the chain, at 40 fs. The latter value is consistent with experimental data for H-bonded complexes.

REFERENCES

1. Wilkinson, A.J., Fersht, A.R., Blow, D.M., and Winter, G., *Biochemistry*, 1993, vol. 22, p. 3581.
2. Krebs, J.F. and Fierke, C.A., *J. Biol. Chem.*, 1993, vol. 268, p. 948.
3. Shan, S., and Herschlag, D., *Proc. Natl. Acad. Sci. USA*, 1996, vol. 93, p. 14474.
4. Zheng, Y.-J. and Bruice, T.C., *Ibid.*, 1997, vol. 94, p. 4285.

5. Lightstone, F.C., Zheng, Y.-J., Maulitz, A.H., and Bruice, .C., *Ibid*., 1997, vol. 94, p. 8417.
6. Hoog, S.S., Smith W.W., Qiu X., et al., *Biochemistry*, 1997, vol. 36, p. 14023.
7. Szilagyi, R.K., Musaev, D.G., and Morokuma, K., *J. Mol. Struct. (Theochem)*, 2000, vol. 506, p. 131.
8. Gigant, B., Charbonnier, J.-B., Eshhar, Z., Green, B.S., and Knossow, M., *Proc. Natl. Acad. Sci. USA*, 1997, vol. 94, p. 7857.
9. Pinto, L.H., Dieckmann, G.R., Gandhi, C.S., et al., *Ibid*., 1997, vol. 94, p. 11301.
10. Oprea, T.I., Hummer, G., and Garcia, A.E., *Ibid*., 1997, vol. 94, p. 2133.
11. Shaltill, S., Cox, S., and Taylor, S.S., *Ibid*., 1998, vol. 95, p. 484.
12. Zheng, Y.-J. and Bruice, T.C., *Ibid*., 1998, vol. 95, p. 4158.
13. Beveridge, A.J., *J. Mol. Struct. (Theochem)*, 1998, vol. 453, p. 275.
14. Davydov, D.R., Hoa, G.H.B., and Peterson, J.A., *Biochemistry*, 1999, vol. 38, p. 751.
15. Yoshioka, Y., Kawai, H., and Yamaguchi, K., *Chem. Phys. Lett*., 2003, vol. 374, p. 45.
16. Nagle, J.F. and Morowitz, H.J., *Proc. Natl. Acad. Sci. USA*, 1978, vol. 75, p. 298.
17. Iwata, S., Ostermeier, C., Ludwig, B., and Michel, H., *Nature*, 1995, vol. 376, p. 660.
18. Pomes, R. and Roux, B., *Biophys. J*., 1998, vol. 75, p. 33.
19. Marx, D., Tuckerman, M.E., Hutter, J., and Parrinello, M., *Nature*, 1999, vol. 397, p. 601.
20. Decornez, H., Drukker, K., and Hammes-Schiffer, S., *J. Phys. Chem. A,* 1999, vol. 103, p. 2891.
21. Sham, Y.Y., Muegge, I., and Warshel, A., *Prot. Struct. Funct. Gen*., 1999, vol. 36, p. 484.
22. Wikstrom, M., *Curr. Opin. Struct. Biol*., 1998, vol. 8, p. 480.
23. Hofacker I. and Schulten, K., *Prot. Struct. Funct. Gen.*, 1998, vol. 30, p. 100.
24. Rastogi, V.K. and Girvin, M.E., *Nature*, 1999, vol. 402, p. 263.
25. Stowell, M.H.B., McPhillips, T.M., Rees, D.C., Soltis, S.M., Abresch, E., and Feher, G., *Science,* 1997, vol. 276, p. 812.
26. Akeson, M. and Deamer, D.W., *Biophys. J*., 1991, vol. 60, p. 101.
27. Dodgson, S.J., Tashian, R.E., Gross, G., and Carter, N.D., *The Carbonic Anhydrases,* New York: Plenum, 1991.
28. Shearer, G.L., Kim, K., Lee, K.M., Wang, C.K., and Plapp, B.V., *Biochemistry*, 1993, vol. 32, p. 11186.
29. Konstantinov, A.A., Siletsky, S., Mitchell, D., Kaulen, A., and Gennis, R.B., *Proc. Natl. Acad. Sci. USA*, 1997, vol. 94, p. 9085.
30. Adelroth, P., Sigurdson, H., Hallen, S., and Brzezinski, P., *Ibid*., 1996, vol. 93, p. 12292.
31. Sagnella, D.E. and Tuckerman, M.E., *J. Chem. Phys.,* 1998, vol. 108, p. 2073.
32. Vuilleumier, R. and Borgis, D., *Ibid*., 1999, vol. 111, p. 4251.
33. Schmitt, U.W. and Voth, G.A., *J. Phys. Chem. B,* 1998, vol. 102, p. 5547.
34. Brewer, M.L., Schmitt, U.W., and Voth, G.A., *Biophys. J*., 2001, vol. 80, p. 1691.
35. Drukker, K., de Leeuw, S.W., and Hammes-Schiffer, S., *J. Chem. Phys*., 1998, vol. 108, p. 6799.
36. Aquist, J. and Warshel, A., *Chem. Rev*., 1993, vol. 93, p. 2523.
37. Mei, H.S., Tuckerman, M.E., Sagnella, D.E., and Klein, M.L., *J. Phys. Chem. B*, 1998, vol. 102, p. 10446.
38. Geissler, P.L., Dellago, C., Chandler, D., Hutter, J., and Parrinello, M., *Science*, 2001, vol. 291, p. 2121.
39. Sadeghi, R.R. and Cheng, H.-P., *J. Chem. Phys.,* 1999, vol. 111, p. 2086.
40. Meuwly, M. and Karplus, M., *Ibid*., 2002, vol. 116, p. 2572.
41. Sagnella, D.E., Laasonen, K., and Klein, M.L., *Biophys. J*., 1996, vol. 71, p. 1172.
42. Pomes, R. and Roux, B., *Ibid*., 2002, vol. 82, p. 2304.
43. Smondyrev, A.M. and Voth, G.A., *Ibid*., 2002, vol. 83, p. 1987.
44. Nemukhin, A., Grigorenko, B.L., Topol, I.A., and Burt, S.K., *J. Phys. Chem. B*, 2003, vol. 107, p. 2958.
45. Cleland, W.W., *Methods Enzymol*., 1995, vol. 249, p. 341.
46. Hirst, J., Duff, J.L.C., Jameson, G.N.L., et al., *J. Am. Chem. Soc*., 1998, vol. 120, p. 7085.
47. Agarwal, P.K., Webb, S.P., and Hammes-Schiffer, S., *Ibid*., 2000, vol. 122, p. 4803.
48. Cui, Q., Elstner, M., and Karplus, M., *J. Phys. Chem.* B, 2002, vol. 106, p. 2721.
49. Yousef, M.S., Fabiola, F., Gattis, J.L., et al., *Acta Crystallographica, Sect. D: Biol. Crystallogr*., 2002, vol. 58, p. 2009.
50. Paddock, M.L., Adelroth, P., Feher, G., Okamura, M.Y., and Beatty, J.T., *Biochemistry*, 2002, vol. 41, p. 14716.
51. Cleland, W.W., *Ibid*., 1992, vol. 31, p. 317.
52. Gerlt, J.A. and Gassman, P.G., *Ibid*., 1993, vol. 32, p. 11943.
53. Gerlt, J.A. and Gassman, P.G., *J. Am. Chem. Soc*., 1993, vol. 115, p. 11552.
54. Cleland, W.W. and Kreevoy, M.M., *Science*, 1994, vol. 264, p. 1887.

55. Frey, P.A., Whitt, S.A., and Tobin, J.B., *Ibid*., 1994, vol. 264, p. 1927.
56. Warshel, A., Papazyan, A., Kollman, P.A., Cleland, W.W., Kreevoy, M.M., and Frey, P.A., *Ibid*., 1995, vol. 269, p. 102.
57. Guthrie, J.P. and Kluger, R., *J. Am. Chem. Soc.,* 1993, vol. 115, p. 11569.
58. Guthrie, J.P., *Chem. Biol*., 1996, vol. 3, p. 163.
59. Warshel, A. and Papazyan, A., *Proc. Natl. Acad. Sci. USA*, 1996, vol. 93. p. 13665.
60. Scheiner, S. and Kar, T., *J. Am. Chem. Soc*., 1995, vol. 117, p. 6970.
61. Aqvist, J. and Warshel, A., *J. Mol. Biol.*, 1992, vol. 224, p. 7.
62. McGrath, M.E., Vasquez, J.R., Craik, C.S., Yang, A.S., Honig, B., and Fletterick, R.J., *Biochemistry*, 1992, vol. 31, p. 3059.
63. Isaev, A.N., *Zh. Fiz. Khim*., 2003, vol. 77, no. 11, p. 2023.
64. Isaev, A.N., *Ibid*., 2005, vol. 79, no. 10, p. 1832.
65. Dimitrova, V., Ilieva, S., and Galabov, B., *J. Mol. Struct. (Theochem),* 2003, vol. 637, p. 73.
66. Foresman, J.B., Keith, T.A., Wiberg, K.B., Snoonian, J., and Frisch, M.J., *J. Phys. Chem*., 1996, vol. 100, p. 16098.
67. *Molecular Interactions,* Ratajczak, H. and Orville-Thomas, W.J., Eds., Chichester: Wiley, 1981.
68. Isaev, A.N. and Hurgin, Yu.I., *Izv. Akad. Nauk SSSR, Ser. Khim*., 1991, no. 4, p. 817.
69. Isaev, A.N., *Zh. Fiz. Khim*., 1993, vol. 67, no. 6, p. 1168.
70. Pinto, L.H., Dieckmann, G.R., Gandhi, C.S., et al., *Proc. Natl. Acad. Sci. USA*, 1997, vol. 94, p. 11301.
71. Mould, J.A., Li, H.-C., Dudlak, C.S., Lear, J.D., Pekosz, A., Lamb, R.A., and Pinto, L.H., *J. Biol. Chem*., 2000, vol. 275, p. 8592.
72. Schweighofer, K.J. and Pohorille, A., *Biophys. J*., 2000, vol. 78, p. 150.
73. Isaev, A., Kar, T., and Scheiner, S., *Int. J. Quantum Chem*., 2007, vol. 108, no. 3, p. 607.
74. Notstrand, B., Vaara, I., and Kannan, K.K., *Isozymes*, Markers, C.L., Ed., New York: Academic, 1975, p. 575.
75. Steiner, H., Jonsson, B.-H., and Lindskog, S., *Eur. J. Biochem*., 1975, vol. 59, p. 253.
76. Silverman, D.N., Tu, C.K., Lindskog, S., and Wynns, G.C., *J. Am. Chem. Soc*., 1979, vol. 101, p. 6734.
77. Silverman, D.N. and Lindskog, S., *Acc. Chem. Res*., 1988, vol. 21, p. 30.
78. Jewell, D.A., Tu, C., Paranawithana, S.R., Tanhauser, S.M., LoGrasso, P.V, Laipis, P.J., and Silverman, D.N., *Biochemistry*, 1991, vol. 30, p. 1484.
79. Kiefer, L.L., Paterno, S.A., and Fierke, C.A., *J. Am. Chem. Soc.*, 1995, vol. 117, p. 6831.
80. Christianson, D.W. and Fierke, C.A., *Acc. Chem. Res.,* 1996, vol. 29, p. 331.
81. Qian, M., Tu, C., Earnhardt, J.N., Laipis, P.J., and Silverman, D.N., *Biochemistry*, 1997, vol. 36, p. 15758.
82. Liang, J.-Y. and Lipscomb, W.N., *Int. J. Quant. Chem.*, 1989, vol. 36, p. 299.
83. Merz, K.M., Jr., Hoffmann, R., and Dewar, M.J.S., *J. Am. Chem. Soc*., 1989, vol. 111, p. 5636.
84. Vedani, A., Huhta, D.W., and Jacober, S.P., *Ibid.,* 1989, vol. 111, p. 4075.
85. Merz, K.M., Jr., *Ibid*., 1991, vol. 113, p. 3572.
86. Jacob, O. and Tapia, O., *Int. J. Quant. Chem*., 1992, vol. 42, p. 1271.
87. Zheng, Y.-J. and Merz, K.M., Jr., *J. Am. Chem. Soc.,* 1992, vol. 114, p. 10498.
88. Lu, D. and Voth, G.A., *Ibid*., 1998, vol. 120, p. 4006.
89. Toba, S., Colombo, G., and Merz, K.M., *Ibid*., 1999, vol. 121, p. 2290.
90. Muguruma, C., *J. Mol. Struct. (Theochem.)*, 1999, vols. 461–462, p. 439.
91. Cui, Q. and Karplus, M., *J. Phys. Chem. B*, 2003, vol. 107, p. 1071.
92. Eriksson, A.E., Jones, T.A., and Liljas, A., *Prot. Struct. Funct. Gen*., 1988, vol. 4, p. 274.
93. Scolnick, L.R. and Christianson, D.W., *Biochemistry*, 1996, vol. 35, p. 16429.
94. Pomes, R. and Roux, B., *Biophys. J*., 1996, vol. 71, p. 19.
95. Lesburg, C.A. and Christianson, D.W., *J. Am. Chem. Soc*., 1995, vol. 117, p. 6838.
96. Venkatasubban, K.S. and Silverman, D.N., *Biochemistry*, 1980, vol. 19, p. 4984.
97. Tu, C.K. and Silverman, D.N., *Ibid*., 1982, vol. 21, p. 6353.
98. Isaev, A. and Scheiner, S., *J. Phys. Chem. B*, 2001, vol. 105, p. 6420.
99. Isaev, A.N., *J. Mol. Struct. (Theochem)*, 2002, vol. 582, p. 195.
100. Pullman, A. and Demoulin, D., *Int. J. Quantum Chem.*, 1979, vol. 16, p. 641.
101. Kannan, K.K., Ramanadham, M., and Jones, T.A., *Ann. N.Y. Acad. Sci*., 1984, vol. 429, p. 49.
102. Nair, S.K. and Christianson, D.W., *J. Am. Chem. Soc*., 1991, vol. 113, p. 9455.
103. Smedarchina, Z., Siebrand, W., Fernandez-Ramos, A., and Cui, Q., *Ibid*., 2003, vol. 125, p. 243.
104. Isaev, A.N., *Zh. Fiz. Khim.*, 2007, vol. 81, no. 6, p. 1058.
105. Ziolek, M., Kubicki, J., Maciejewski, A., et al., *Chem. Phys. Lett.,* 2003, vol. 369, p. 80.